BMC Cancer

RESEARCH

Open Access

ANKRD49 promotes the metastasis of NSCLC via activating JNK-ATF2/c-Jun-MMP-2/9 axis

Jia Sun[1,2†], Jin-rui Hu[3†], Chao-feng Liu[1†], Yuan Li[4], Wei Wang[3], Rong Fu[3], Min Guo[5], Hai-long Wang[3*] and Min Pang[1,6*]

Abstract

Background Ankyrin repeat domain 49 (ANKRD49) has been found to be highly expressed in multiple cancer including lung adenocarcinoma (LUAD) and lung squamous carcinoma (LUSC). However, the function of ANKRD49 in the pathogenesis of NSCLC still remains elusive. Previously, ANKRD49 has been demonstrated to promote the invasion and metastasis of A549 cells, a LUAD cell line, via activating the p38-ATF-2-MMP2/MMP9 pathways. Considering the heterogeneity of tumor cells, the function and mechanism of ANKRD49 in NSCLC need more NSCLC-originated cells to clarify.

Methods Real-time qPCR was employed to test ANKRD49 expression levels in nine pairs of fresh NSCLC tissues and the corresponding adjacent normal tissues. The function of ANKRD49 was investigated using overexpression and RNA interference assays in lung adenocarcinoma cell line (NCI-H1299) and lung squamous carcinoma cell line (NCI-H1703) through gelatin zymography, cell counting kit-8, colony formation, wound healing, migration and invasion assays mmunoprecipitation was performed to in vitro. Immunoprecipitation was performed to test the interaction of c-Jun and ATF2. Chromatin immunoprecipitation was conducted to assess the transcriptional regulation of ATF2/c-Jun on MMP-2/9. Moreover, the tumorigenicity of ANKRD49 was evaluated in nude mice models and the involved signal molecular was also measured by immunohistochemical method.

Results We found that the levels of ANKRD49 in cancerous tissues were higher than those in adjacent normal tissues. in vitro assay showed that ANKRD49 promoted the migration and invasion of NCI-H1299 and NCI-H1703 cells via enhancing the levels of MMP-2 and MMP-9. Furthermore, ANKRD49 elevated phosphorylation of JNK and then activated c-Jun and ATF2 which interact in nucleus to promote the binding of ATF2:c-Jun with the promoter MMP-2 or MMP-9. In vivo assay showed that ANKRD49 promoted lung metastasis of injected-NSCLC cells and the high metastatic rate was positively correlated with the high expression of ANKRD49, MMP-2, MMP-9, p-JNK, p-c-Jun and p-ATF2.

Conclusion The present study indicated that ANKRD49 accelerated the invasion and metastasis of NSCLC cells via JNK-mediated transcription activation of c-Jun and ATF2 which regulated the expression of MMP-2/MMP-9. The

†Jia Sun, Jin-Rui Hu and Chao-feng Liu contributed equally to this work.

*Correspondence:
Hai-long Wang
longwty@163.com
Min Pang
pangmin2009@126.com

Full list of author information is available at the end of the article

molecular mechanisms of ANKRD49's function is different from those found in A549 cells. The current study is a supplement and improvement to the previous research.

Keywords ANKRD49, Matrix metalloproteinases, ATF2, c-Jun, Metastasis

Introduction

Lung carcinoma is the most common cause of cancer-related deaths globally, with an estimated 1.6 million deaths annually [1]. Non-small cell lung cancer (NSCLC) accounts for 85% of all cases [2], of which lung adenocarcinoma (LUAD) and lung squamous cell carcinoma (LUSC) are the most common subtypes [3]. Notwithstanding unprecedented advances in the remedy of NSCLC, such as targeted therapy and immunotherapy, have been made in recent years, the long-term prognosis of NSCLC patients remains poor, with a 5-year survival rate of less than 15% [4, 5]. Therefore, it is essential to clarify the molecular pathogenesis of NSCLC and identify more precise prognostic markers and therapeutic targets.

The ankyrin repeat domain consists of 30~34 amino acid residues and mediates protein-protein interactions. ANKRD49 (ankyrin repeat domain 49) contains four ankyrin motifs. ANKRD49 is highly expressed in the testes and is involved in spermatogenesis [6, 7]. ANKRD49 also participates in the progression of malignant gliomas and gastric cancer in humans [8, 9]. Previously, we explored the expression pattern of ANKRD49 protein in NSCLC (80 cases of LUAD and 80 cases of LUSC) and found that the levels of ANKRD49 in cancer tissues were higher than those in tumor-adjacent normal tissues, its expression correlated with the TNM (tumor-node-metastasis) stage, distal metastasis, lymph node metastasis and differentiation [10]. Moreover, patients with higher ANKRD49 showed lower OS (overall survival) rate and higher ANKRD49 expression in lung tissues may serve as an independent prognostic marker for NSCLC patients [10, 11]. Howbeit, the function and underlying mechanisms of ANKRD49 in NSCLC has not yet been fully elucidated.

ANKRD49 has been demonstrated to promote the invasion and metastasis of A549 cells, a lung adenocarcinoma cell line, via activating the p38/ATF-2 signaling pathway and then elevating the levels of MMP2/MMP9 in our previous study [11]. Considering the heterogeneity of tumor cells, the function and mechanism of ANKRD49 in NSCLC need more NSCLC-originated cells to clarify. Therefore, in the present study, another LUAD cell line (NCI-H1299) and a LUSC cell line (NCI-H1703) were selected and our findings illustrated that ANKRD49 accelerated the migration and invasion of NCI-H1299 and NCI-H1703 cells via the JNK-ATF2/c-Jun-MMP-2/MMP-9 pathway, unlike its function in A549 cells.

Materials and methods

Human tissue samples

Nine pairs of fresh NSCLC tissues and the corresponding adjacent normal tissues were collected from patients who underwent surgery at the First Hospital of Shanxi Medical University from October 2020 to December 2020. No patients in this study received other treatment before surgery.

Cell lines and cells culture

The human bronchial epithelial cell line (HBEC) and NSCLC cell lines H1299, A549, H446, H460, Calu-3, H1703, sk-MES-1 were obtained from the Cell Culture Center of the Chinese Academy of Medical Sciences (Beijing, China). These NSCLC cell lines were cultured in Advanced RPMI 1640 medium (Seven, Beijing, China) supplemented with 10% fetal bovine serum (Every Green, Zhejiang, China) and incubated at 37 °C in 5% CO_2.

Establishment of ANKRD49 stably expressed cell lines

H1299 and H1703 cells were infected with lentivirus-5 ANKRD49 or lentivirus-3 ANKRD49-shRNA and corresponding vectors (Gene Pharma, Shanghai, China) according to the manufacturer's protocols to construct the stable ANKRD49 overexpression (ANKRD49-OE) or ANKRD49 knockdown (ANKRD49-sh) groups. Meanwhile, the controls for overexpression (LV5) and knockdown (LV3) were also established. After infection of lentivirus, cells were incubated for more than 48 h and puromycin (2 μg/ml) was added to screen the stable cells. LV3 and ANKRD49-sh sequences were listed in Supplementary Table 1.

Reagents and antibodies

Puromycin (P816466) was purchased from MACKLIN (Shanghai, China). Anisomycin (GC11559) was purchased from GLPBIO (Shanghai, China). The p38 mitogen-activated protein kinase (MAPK) inhibitor (HY-10,256, SB203580) and JNK inhibitor (HY-12,041, SP600125) were purchased from MedChemExpress (New Jersey, USA). MMPs inhibitor (SF4180, ilomastat) was purchased from Beyotime Biotechnology (Shanghai, China). Rabbit anti-ANKRD49 primary antibody (Proteintech, Cat# 25034-1-AP, RRID:AB_2879860), rabbit anti-MMP-2 polyclonal antibody (Cat# bs-4599R, RRID:AB_11083963), rabbit anti-MMP-9 polyclonal antibody (Cat# bs-0397R, RRID:AB_10853038), rabbit anti-c-Jun polyclonal antibody (Cat# bs-0670R, RRID:AB_10857880), rabbit anti-p-ATF2 polyclonal

antibody (Cat# bs-3033R, RRID:AB_10883830) and Alexa Fluor® 488-conjugated goat anti-rabbit IgG (Cat# bs-0295G-A488, RRID:AB_10893781) were obtained from Bioss Biotechnology (Beijing, China). The mouse anti-p-c-Jun monoclonal antibody (Cat# 558,036, RRID: AB_2249448) was obtained from BD Biosciences (New Jersey, USA). Rabbit anti-p38 monoclonal antibody (Cat# 8690, RRID: AB_10999090), rabbit anti-p-p38 monoclonal antibody (Cat# 4511, RRID: AB_2139682), rabbit anti-ERK monoclonal antibody (Cat# 4695, RRID: AB_390779), rabbit anti-p-ERK monoclonal antibody (Cat# 4376, RRID: AB_331772), rabbit anti-SAPK/JNK monoclonal antibody (Cat# 9258, RRID: AB_2141027), and rabbit anti-p-JNK monoclonal antibody (Cat# 4668, RRID: AB_823588) were purchased from Cell Signaling Technology (Danvers, MA, USA). Rabbit anti-ATF2 polyclonal antibody (Cat# BS1022, RRID: AB_1664115), rabbit anti-β-actin polyclonal antibody (Cat# AP0060, RRID: AB_2797445), rabbit anti-GAPDH polyclonal antibody (Cat# AP0063, RRID: AB_2651132), rabbit anti-Histone-H3 polyclonal antibody (Cat# BS7675), rabbit anti-PARP polyclonal antibody (Cat# BS7190), and rabbit anti-β-tubulin polyclonal antibody (Cat# AP0064, RRID: AB_2797447) were acquired from Bioworld (Minnesota, USA). Rabbit anti-ATF2 polyclonal antibodies (Cat# D155200) and rabbit anti-p-ATF2 polyclonal antibodies (Cat# D155010) were purchased from Sangon Biotech (Shanghai, China). Anti-rabbit IgG (H+L) (Cat# BA1050, RRID: AB_2904507) and anti-mouse IgG (H+L) (Cat# BA1054, RRID: AB_2734136) were purchased from Boster Biological Technology (Wuhan, China). Dylight 649 and goat anti-mouse IgG (Cat# 610-143-002, RRID: AB_11182582) were obtained from Rockland (Philadelphia, USA).

Western blot

Total protein from cells or tissues was extracted using SDS lysis buffer containing 2% SDS, 10% glycerol, and 50 mM Tris-HCl (pH 6.8), and quantified using the Enhanced BCA Protein Assay Kit (Beyotime Biotechnology). Proteins (30 μg) were loaded onto a 12% SDS-PAGE gel, separated, and transferred onto polyvinylidene fluoride (PVDF) membranes. The membranes were blocked using 5% skimmed milk, followed by probing with the indicated primary antibodies at 4 °C overnight, and then incubated with an anti-rabbit/mouse HRP-conjugated IgG at room temperature for 1 h. Blots were developed using the ECL kit (Seven, Beijing, China) and detected using the ChemiDoc imaging system (Bio-Rad, California, USA).

Real-time qPCR analyses

Total RNA from NSCLC cells, nine pairs of human NSCLC tissues, and matched adjacent normal tissues were prepared using the Total RNA Extraction Kit (Promega, Madison, WI, USA) following the manufacturer's instructions. RT-qPCR was performed using the RT-PCR Kit (Seven, Beijing, China) on the Quant Studio 3 (Thermo Fisher Scientific, Massachusetts, USA), according to the manufacturer's procedures. All the primers are listed in Supplemental Table 2. β-actin was used as the control, and the relative mRNA expression was defined using the $2^{-\Delta\Delta Ct}$ method.

Gelatin zymography

MMP-2 and MMP-9 activities were evaluated using gelatin zymography. 5×10^5 cells were pretreated with serum-free medium for 48 h. The medium was collected, centrifuged at 1,500× g for 15 min at 4 °C, and mixed with non-reducing sample buffer for electrophoresis on a polyacrylamide gel containing 0.1% (w/v) gelatin. Proteolysis was assessed as a white zone in the dark blue fields. The 62 kDa and 92 kDa bands corresponded to active MMP-2 and MMP-9, respectively. The gelatinase activity of MMP-2 and MMP-9 was illustrated via the area of the clear zone in the dark blue gel and analyzed using ImageJ analysis software (National Institute of Health, Maryland, USA).

Cell counting kit-8 (CCK-8) assay

The CCK-8 assay was performed to evaluate cellular proliferation, according to the manufacturer's protocols. Briefly, ANKRD49-OE or LV5 H1299 cells, ANKRD49-sh, or LV3 H1703 cells were cultured in 96-well plates at a density of 1×10^3 cells per well in a 5% CO_2 incubator at 37 °C. Next, 100 μl serum-free medium containing 10 μl CCK-8 reagent (Seven, Beijing, China) was added to each well, followed by another 1 h incubation. The absorbance of the cells was measured at 450 nm using a microplate reader (Molecular Devices, California, USA).

Colony formation assay

ANKRD49-OE or LV5 H1299 cells, ANKRD49-sh, or LV3 H1703 cells were plated in six-well plates at a density of 5×10^2 cells/well and cultured at 37 °C for 1 week. After washing with PBS, the cells were fixed with methanol and stained with 0.1% crystal violet solution. The colonies were photographed and quantified using a light microscope (Eclipse Ts2; Nikon, Tokyo, Japan).

Wound healing assay

Cells (2×10^5) were seeded into six-well plates and cultured for 24 h. Wounds in the confluent cells were created using a 200 μl pipette tip, followed by washing the cells with PBS to remove any floating cells. Next, complete medium was added and the wound margins were photographed. Subsequently, wound healing was photographed at 24 and 48 h using a Nikon photomicroscope

(Eclipse Ts2, Nikon, Tokyo, Japan). Migratory ability was calculated by measuring the distance between different groups of cells simultaneously.

Migration and invasion assays

Cells (2×10^4) were seeded into the upper chamber of 24-well inserts (8.0 μm, Corning, California, USA). The upper chamber was pre-coated with Matrigel (BD Biosciences, California, USA), and a medium containing 10% FBS was added to the lower chamber for the invasion assay. After incubation at 37 °C for 24 h, the remaining cells in the upper chamber were scraped off and the cells on the lower side of the chamber were fixed, stained, and viewed using a Nikon photomicroscope (Eclipse Ts2). Data were analyzed by counting at least five random fields.

Cytoplasmic and nuclear protein extraction

ANKRD49-OE or LV5 H1299 cells were plated in 10 cm plates at a density of 5×10^6 cells/plate and cultured at 37 °C for 2 days. The subcellular proteins in ANKRD49-OE or LV5 H1299 cells were prepared using a subcellular structure cytoplasm and nucleus extraction kit (Bioss Biotechnology). In brief, samples were centrifuged at 750 × g for 5 min at 4 °C. The supernatant was collected and centrifuged at 3400, × g, 10 min (cytoplasmic fraction). This process was repeated four times to remove nuclear contamination. The pellet was washed with fractionation buffer and centrifuged at 750 × g, 5 min to remove cytoplasmic contamination at least three times. The nuclear/membrane fraction was dissolved in RIPA buffer. The protein samples (20 μg) were subjected to Western blot with p-ATF2 or p-c-Jun antibodies.

Immunofluorescence

H1299 cells were transfected with pMSCVpuro-ANKRD49 or the vector for 48 h, and 5×10^4 cells were seeded onto sterile coverslips in a twelve-well plate for another 24 h. The medium was removed, and cells were fixed with 4% paraformaldehyde and then permeabilized with 0.01% Triton X-100 at room temperature for 10 min. Cells were incubated with anti-p-ATF2 antibody or anti-p-c-Jun antibody at 4 °C overnight, and then probed with Alexa Fluor® 488-conjugated goat anti-rabbit IgG or Dylight 649 goat anti-mouse IgG at room temperature for 1 h in darkness. Nuclei were stained with DAPI (Beyotime) for 5 min, and fluorescence signals were observed using a fluorescence microscope (Eclipse Ts2).

Co-immunoprecipitation (Co-IP)

Nucleus proteins of the ANKRD49-OE or LV5 H1299 cells (1×10^6) were extracted and 25 μg of them were precleared using Protein A/G Agarose (Santa Cruz, California, USA). Subsequently, 2 μl rabbit anti-ATF2 or normal rabbit IgG was added to the lysates and incubated at 4 °C for 12 h. Next, 20 μl of Protein A/G PLUS Agarose was mixed into the lysates and incubated at 4 °C overnight. Agarose was washed three times using wash buffer, and the bound proteins were separated by SDS-PAGE.

Chromatin immunoprecipitation assay

The chromatin immunoprecipitation (CHIP) assay was conducted in accordance with the manufacturer's protocols (Beyotime Biotechnology). The binding site of ATF2/c-Jun in the MMP-2 or MMP-9 promoter region and the position of the CHIP primers are illustrated in Supplementary Fig. S1. Chromatin solutions were sonicated and incubated with anti-p-ATF2, anti-p-c-Jun, or control IgG at 4 °C for 12 h. DNA-protein cross-links were reversed, and chromatin DNA was subsequently purified and subjected to PCR analysis. Primers for amplifying the MMP-2 or MMP-9 promoter, which contains the binding site of ATF2/c-Jun, are listed in Supplementary Table 3. The immunoprecipitated DNA was analyzed by qPCR. The qPCR products were resolved on a 1.2% agarose gel and visualized by nucleic acid dye staining.

Mouse xenograft and metastasis models

Ten female BALB/c nude mice and ten male BALB/c nude mice (5~6-week-old) were obtained from the Experimental Animal Center of Shanxi Medical University. The mice were housed under SPF conditions with a 12 h light-dark cycle and ad libitum access to food and water at 23 °C with 60% humidity. Female mice were randomly allocated to either LV5 (n=5) or ANKRD49-OE H1299 cells (n=5). Male mice were randomly allocated to either LV3 (n=5) or ANKRD49-sh H1703 cells (n=5). One week of acclimation, 4×10^6 cells in 200 μl saline were injected into the lateral tail veins of the nude mice. After the injection, the health of the mice was monitored daily. After 4 weeks, the mice were sacrificed, and whole lungs were collected to count the metastatic nodules on the surface. Lung tissues were fixed in 10% paraformaldehyde for further hematoxylin-eosin (H&E) staining and IHC analysis. All animal experiments were approved by the Animal Ethics Committee of the Shanxi Medical University (approval number SYDL-2020016) and was performed according to the procedures that complied with the ARRIVE guidelines.

Immunohistochemistry (IHC)

Five micrometer-thick sections of formalin-fixed paraffin-embedded lung tissues from nude mice were prepared for IHC staining. Slides were deparaffinized, rehydrated, and microwaved for antigen retrieval in 0.01 M, PH 6.0 sodium citrate buffer. Endogenous peroxidase activity was blocked using 3% H_2O_2. Subsequently, sections were incubated with the corresponding primary

antibody (1:100) for 45 min at room temperature. Diaminobenzidine (DAB) (Boster, Wuhan, China) was used to visualize peroxidase activity. The immunostaining intensity of ANKRD49, NAPSA, NKX2-1, MMP-2, MMP-9, p63, p-JNK, p-c-Jun, and p-ATF2 was calculated according to the published *H*-score method: *H*-score value = (unstained tumor cells) % × 0 + (weakly stained tumor cells) % × 1 + (moderately stained tumor cells) % × 2 + (strongly stained tumor cells) % × 3.

Statistical analysis

Correlations between the level of ANKRD49 and the levels of MMP-2, MMP-9, p-JNK, p-ATF2, and p-c-Jun were analyzed using Pearson's correlation coefficient. A strong correlation was defined as an *r*-value of ≥0.5. SPSS18.0 (IBM, Inc) and GraphPad Prism7.0 (GraphPad Software Inc.) software were used to analyze the data. The analyses were repeated in triplicate. Quantitative data are expressed as the mean ± standard deviation (SD) and analyzed using a Student's t-test or one-way analysis of variance followed by Tukey's post hoc test using GraphPad Prism software. A two-sided *P*-value < 0.05 was considered to indicate a statistically significant difference.

Results

ANKRD49 is highly expressed in NSCLC

To investigate the expression pattern of ANKRD49 in fresh tissues from NSCLC, nine fresh tumor tissues and adjacent normal tissues (6 cases of LUAD and 3 cases of LUSC) were collected and the ANKRD49 mRNA was measured using RT-qPCR. The data showed that the expression of ANKRD49 mRNA in tumor tissues was significantly higher than that in adjacent normal tissues (Fig. 1A). Next, the expression of ANKRD49 mRNA in human bronchial epithelial cell line (HBEC), as well as in five LUAD lines (H1299, A549, H446, H460, Calu-3) and two LUSC lines (H1703, sk-MES-1) was assessed by RT-qPCR. The results demonstrated that the expression of ANKRD49 was obviously higher in H1299, A549, H446, H1703, and sk-MES-1 cells than in the human bronchial epithelial cell line (Fig. 1B). Accordingly, H1299 cell line was selected for ANKRD49 overexpression assay, while H1703 cell line was opted for ANKRD49 knockdown analysis.

ANKRD49 promotes the migration and invasion of H1299 cells

To investigate the function of ANKRD49 in LUAD cells, we established stable ANKRD49-OE or ANKRD49-sh H1299 cells, as well as their respective control cells LV5 and LV3. RT-qPCR and Western blot assays showed that ANKRD49-OE and ANKRD49-sh H1299 cells were constructed (Fig. 2A, B). CCK-8 and colony formation assays revealed that ANKRD49 had no effect on H1299 cell proliferation (Supplementary Fig. S2). Wound healing, transwell migration, and invasion assays illustrated that ANKRD49-OE markedly enhanced the migration and invasion of H1299 cells compared to the LV5 group, and the opposite results were observed in the ANKRD49-sh cells compared to the LV3 group (Fig. 2C-F). Herein, we wanted to know whether endogenous levels of ANKRD49 correlated with differential endogenous migration/invasion potential, wound healing, transwell migration and invasion assays were performed using H1703 cells (higher expression of ANKRD49) and H1299 cells (lower expression of ANKRD49). The results exhibited that H1703 cells had the higher capability in cellular migration and invasion than those in H1299 cells (Supplementary Fig. S3). Taken together, these data demonstrated that ANKRD49 accelerated the migration and invasion of H1299 and 1703 cells.

ANKRD49 upregulates MMP-2/MMP-9 expression by activating the MAPK pathway in H1299 cells

The high expression of MMP-2 and MMP-9 in cancerous tissues has been correlated with tumor cell matrix degradation, invasion, and migration [12–14]. To uncover the molecular basis of ANKRD49 on invasion and migration, the expression of MMP-2 and MMP-9 was tested when ANKRD49 was overexpressed or downregulated by RT-qPCR and Western blot assays. The results revealed that MMP-2 and MMP-9 levels were elevated in ANKRD49-OE and attenuated in ANKRD49-sh H1299 cells compared with the LV5 and LV3 groups, respectively (Fig. 3A, B). Next, the gelatinase activities of MMP-2 and MMP-9 were markedly boosted in ANKRD49-OE H1299 cells and declined in ANKRD49-sh H1299 cells, compared with those in the LV5 and LV3 groups, respectively (Fig. 3C, D). In order to confirm whether the effect of ANKRD49 was dependent on MMP-2 and MMP-9, ANKRD49-OE H1299 cells were pretreated with 10 μM ilomastat (MMP inhibitor) for 1 h. and the wound healing assay displayed that inhibition of MMP-2/MMP-9 attenuated the migration and invasion of H1299 cells (Fig. 3E, F).

It is well established that mitogen-activated protein kinases (MAPKs), including p38 MAPK, ERK, and JNK, are involved in tumor metastasis and invasion [15–17]. As illustrated in Fig. 4A, the levels of p-p38 and p-JNK were obviously augmented in ANKRD49-OE and decreased in ANKRD49-sh H1299 cells compared with the LV5 and LV3 groups, respectively, while the levels of p-ERK were not altered. Next, p38 MAPK inhibitor (10μM SB203580), JNK inhibitor (10μM SP600125), or DMSO (10 μL) was used to pretreat ANKRD49-OE H1299 cells for 1 h. We found that SP600125 significantly decreased MMP-2/MMP-9 levels compared to DMSO-treated cells, whereas SB203580 had no effect

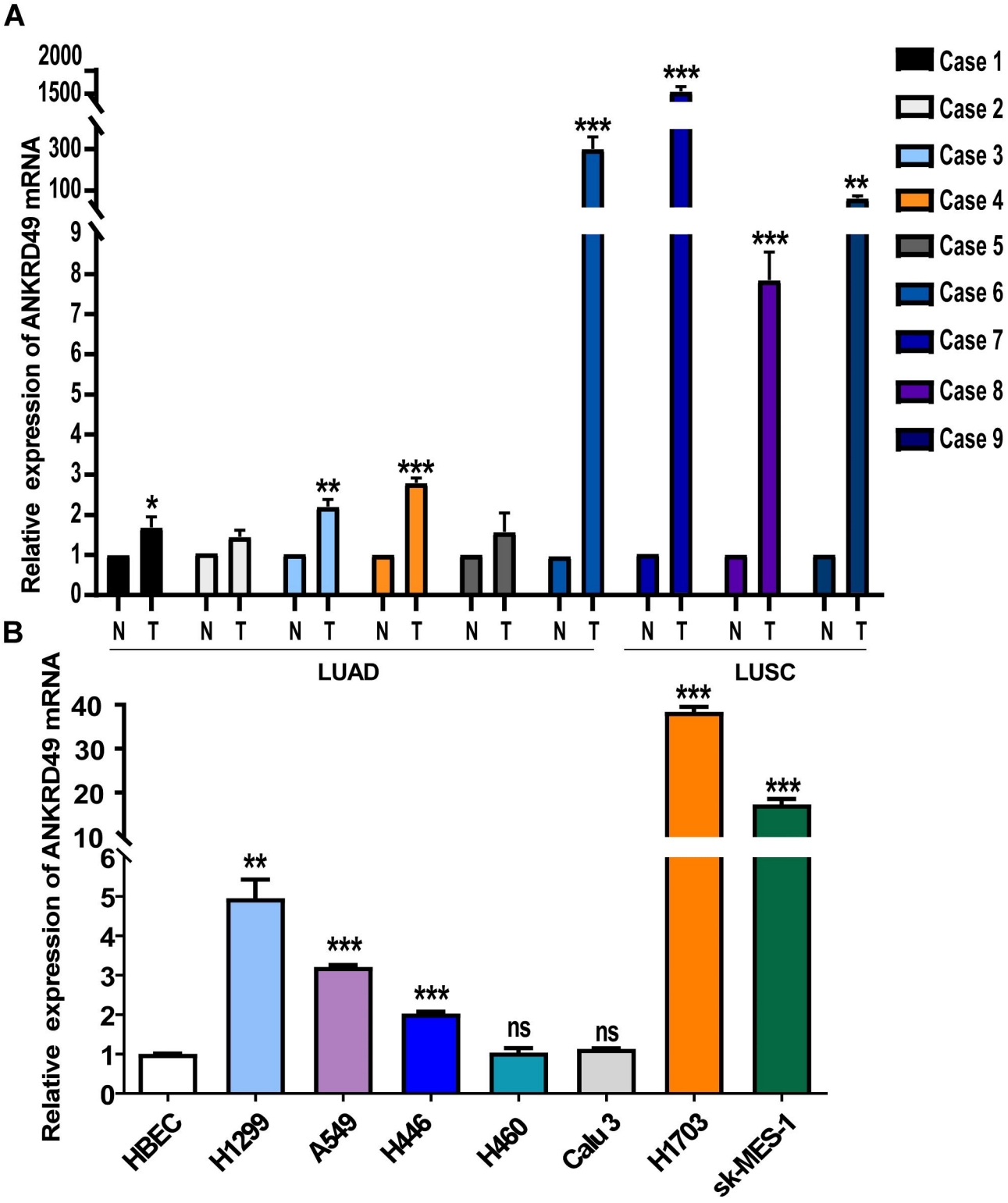

Fig. 1 ANKRD49 is upregulated in NSCLC. (**A**) The mRNA levels of ANKRD49 in nine fresh NSCLC tissues and corresponding adjacent normal tissues were analyzed by RT-qPCR (N: normal tissues; T: tumorous tissues). (**B**) The mRNA levels of ANKRD49 were assessed by RT-qPCR in the human bronchial epithelial cell line (HBEC) and seven NSCLC cell lines. Data are expressed as means ± standard deviation. ns, not significant, $^{*}P < 0.05$, $^{**}P < 0.01$, $^{***}P < 0.001$ vs. corresponding adjacent normal lung tissues or HBEC cells

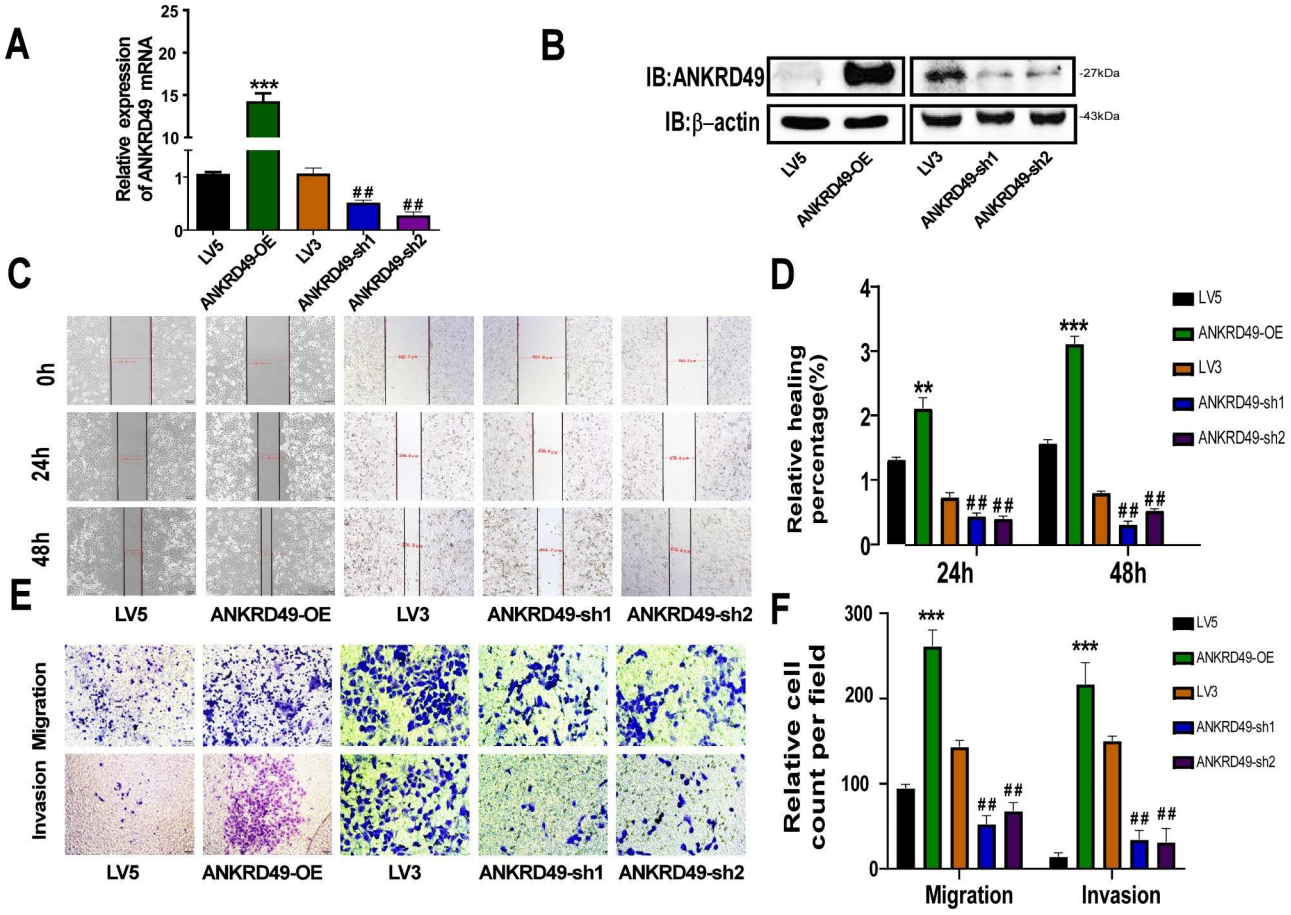

Fig. 2 ANKRD49 potentiates migration and invasion of H1299 cells. (**A**, **B**) Identification of ANKRD49-OE or ANKRD49-sh H1299 cells was validated by RT-qPCR and Western blot. (**C**, **D**) Wound healing assay was used to measure migration of ANKRD49-OE and ANKRD49-sh H1299 cells, representative images were taken at a magnification of 40×, at 0, 24 and 48 h. (**E**, **F**) Transwell migration and invasion assays were performed to detect migration and invasion of ANKRD49-OE and ANKRD49-sh H1299 cells. Representative images were taken at 200× magnification. Statistical analysis from five random fields was conducted. All experiments were repeated independently three times. Data are expressed as means ± standard deviation. $^{*}P<0.05$, $^{**}P<0.01$, $^{***}P<0.001$ vs. LV5 group, $^{\#}P<0.05$, $^{\#\#}P<0.01$ vs. LV3 group

on MMP-2/MMP-9 expression (Fig. 4B, C). Besides, the wound healing assay also exhibited that inhibition of JNK abated the migration and invasion of ANKRD49-OE H1299 cells, whereas inhibition of p38 had no effect on migration and invasion of ANKRD49-OE H1299 cells (Fig. 4D, E). To explore the specific role of JNK on MMP-2/MMP-9 expression, p-ATF2 and p-c-Jun, which are regulatory targets of JNK [18], were analyzed by Western blot. As shown in Fig. 4F, the levels of p-ATF2 and p-c-Jun were both boosted in ANKRD49-OE and weakened in ANKRD49-sh H1299 cells compared with the LV5 and LV3 groups, respectively. Since ATF2 also has been reported to be regulated by p38 MAPK [19], in order to clarify whether p38 MAPK was involved in the regulation of ATF2 in ANKRD49-OE settings, SP600125 or SB203580 was used and p-ATF2 was analyzed. The results illustrated that SP600125 decreased the level of p-ATF2, but SB203580 did not (Fig. 4G, H), indicating that p38 MAPK didn't participate in the regulation of ATF2 in ANKRD49-OE H1299 cells. Overall, these data demonstrate that ANKRD49 promotes the invasion and migration of H1299 cells by enhancing MMP-2/MMP-9 expression mediated by the JNK but not p38 MAPK pathway.

ANKRD49 activates ATF2/c-Jun transcription factor as a heterodimer to regulate MMP-2/MMP-9 expression in H1299 cells

ATF2 and c-Jun belong to the AP-1 family [20], translocate into the nucleus, and regulate the expression of target genes, including MMPs [21, 22]. Accordingly, the nuclear distribution of p-ATF2 and p-c-Jun was measured. The results showed that the nuclear levels of ATF2 and c-Jun as well as their phosphorylation were significantly enhanced in ANKRD49-OE H1299 cells compared to those in the LV5 group (Fig. 5A, B). It is widely acknowledged that ATF2 contains a nuclear export signal (NES) in its leucine zipper region and two nuclear

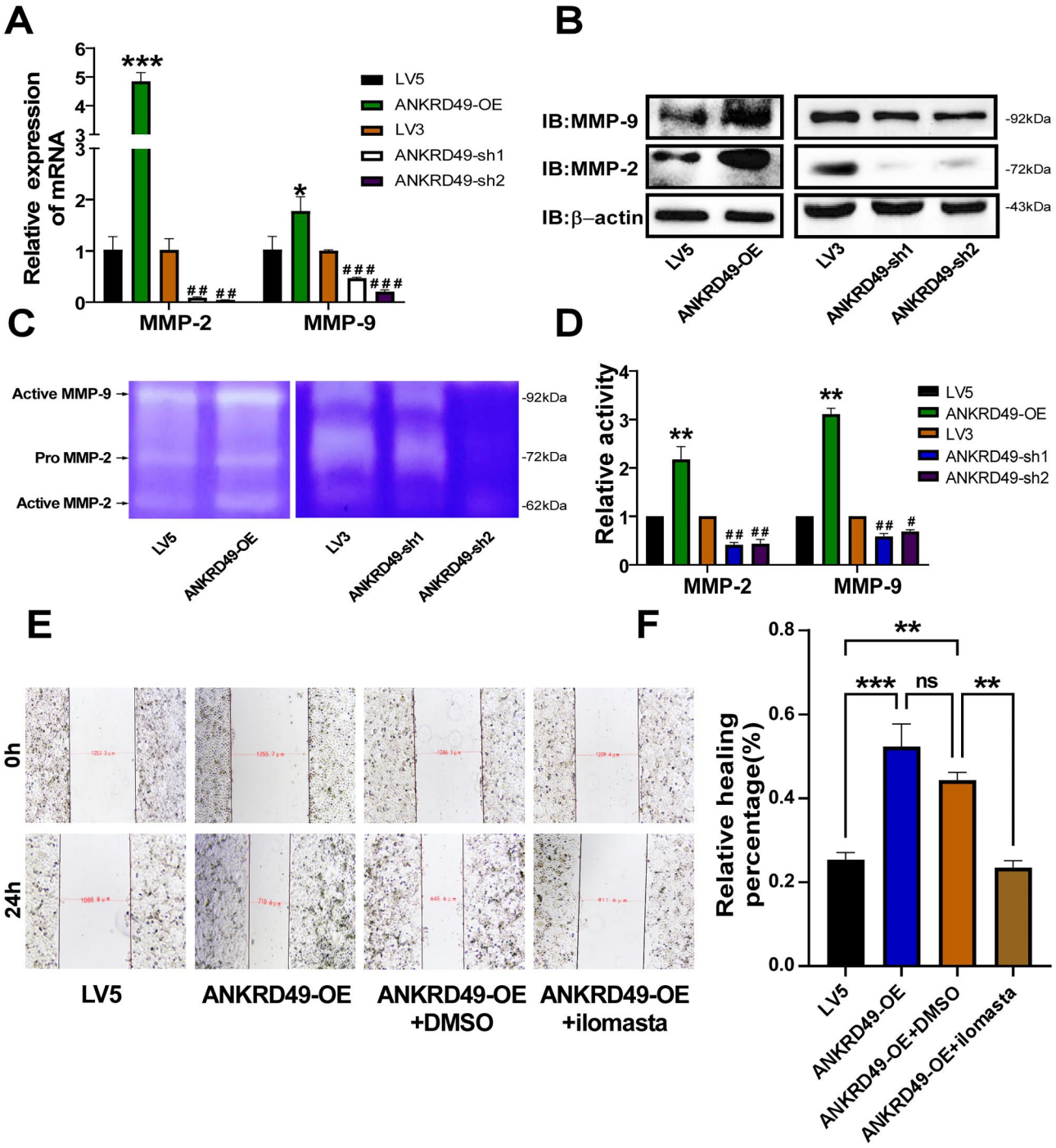

Fig. 3 ANKRD49 upregulates MMP-2/MMP-9 expression in H1299 cells. (**A**, **B**) The mRNA and protein levels of MMP-2 and MMP-9 in ANKRD49-OE and ANKRD49-sh H1299 cells were detected using RT-qPCR and Western blot assays. (**C**, **D**) The activity of MMP-2 and MMP-9 in ANKRD49-OE and ANKRD49-sh H1299 cells was detected by gelatin zymography. (**E**, **F**) A wound healing assay was conducted to assess the effect of MMPs inhibitor (ilomastat) on the migration of ANKRD49-OE H1299 cells; representative images were taken at 40× magnification at 0 and 24 h. Data are expressed as means ± standard deviation. $^{*}P<0.05$, $^{**}P<0.01$, $^{***}P<0.001$ vs. LV5 group, $^{\#}P<0.05$, $^{\#\#}P<0.01$ vs. LV3 group

localization signals (NLS) in its basic region, leading to continuous shuttling between the nucleus and the cytoplasm [23]. It is essential for ATF2's transcriptional activation that ATF2 dimerizes with c-Jun in the nucleus which prevents the export of ATF2 [24]. Co-immunoprecipitation assay revealed that ANKRD49 promoted the interaction between p-ATF2 and p-c-Jun in the nucleus (Fig. 5C). In addition, immunofluorescence assay also

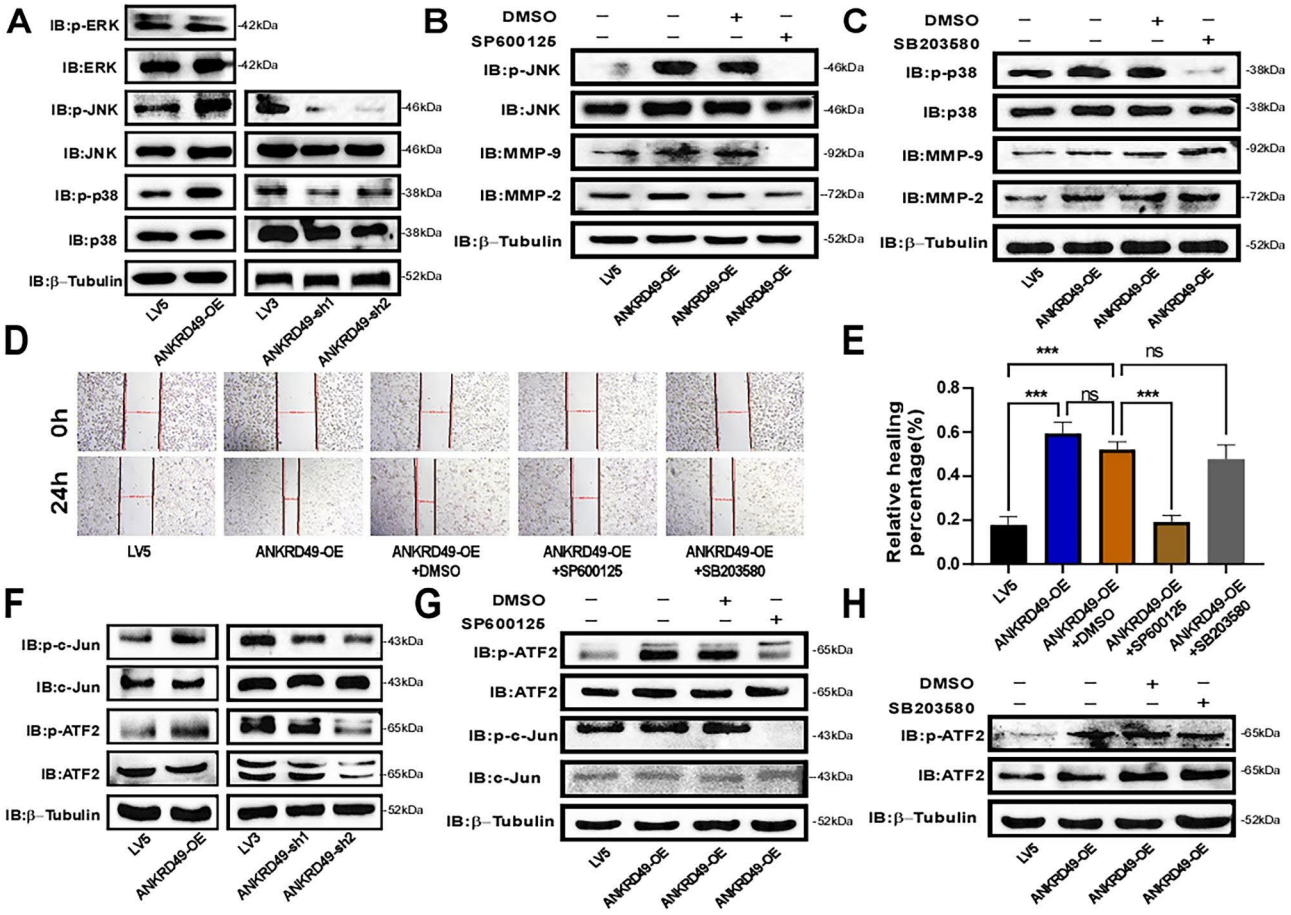

Fig. 4 ANKRD49 activates JNK pathway to regulate the expression of MMP-2/MMP-9 in H1299 cells. (**A**) The MAPK protein levels in ANKRD49-OE and ANKRD49-sh H1299 cells were assessed by Western blot. (**B**, **C**) The effects of JNK inhibitor or p38 MAPK inhibitor on the levels of MMP-2/MMP-9 in ANKRD49-OE H1299 cells were tested by Western blot. β-Tubulin served as an internal control. (**D**, **E**) A wound healing assay was conducted to assess the effect of JNK inhibitor (SP600125) or p38 inhibitor (SB203580) on the migration of ANKRD49-OE H1299 cells; representative images were taken at 40× magnification at 0 and 24 h. (**F**) The levels of p-ATF2 and p-c-Jun in ANKRD49-OE and ANKRD49-sh H1299 cells were measured by Western blot. (**G**, **H**) The levels of p-ATF2 and p-c-Jun in ANKRD49-OE H1299 cells treated with SP600125, SB203580 or DMSO were detected by Western blot. Data are expressed as means ± standard deviation. $^{*}P < 0.05$, $^{**}P < 0.01$, $^{***}P < 0.001$ vs. LV5 group

showed that ANKRD49 promoted the nuclear co-localization of p-ATF2 and p-c-Jun (Fig. 5D). Furthermore, chromatin immunoprecipitation assay was conducted to analyze the binding ability of ATF2 or c-Jun to the MMP-2 or MMP-9 promoter region. Our results illustrated that ANKRD49 enhanced the binding of ATF2 or c-Jun to the MMP-2 or MMP-9 promoter region (Fig. 5E-G). Taken together, these findings suggest that ANKRD49 activates ATF2/c-Jun transcription factor as a heterodimer to regulate MMP-2/MMP-9 expression in H1299 cells.

ANKRD49 promotes migration and invasion of H1703 cells via MMP-2/MMP-9 mediated by JNK-ATF2/c-Jun pathway

Furthermore, the function of ANKRD49 in LUSC was investigated by establishing stable ANKRD49 knockdown (ANKRD49-sh) H1703 cells and a corresponding control LV3. RT-qPCR and Western blot assays demonstrated that ANKRD49-sh H1703 cells were successfully prepared (Fig. 6A, B). CCK-8 and colony formation assays revealed that ANKRD49 had no effect on H1703 cells' proliferation (Supplementary Fig. S4). Wound healing, transwell migration, and invasion tests exhibited that ANKRD49-sh dramatically attenuated the migration and invasion of H1703 cells compared to the LV3 group (Fig. 6C-F). Additionally, we found that downregulation of ANKRD49 diminished both the expression and activity of MMP-2 and MMP-9 (Fig. 7A-D). Similarly, downregulation of ANKRD49 reduced the levels of p-JNK, p-p38, p-ATF2, and p-c-Jun in H1703 cells (Fig. 7E, F). To further confirm whether the effect of ANKRD49 on the MMP-2/MMP-9 levels in H1703 cells was dependent on JNK pathway just like it's function in H1299cells, Anisomycin (20μM), an activator of JNK and p38 MAPK [25] was used to pretreat ANKRD49-sh H1703 cells for 1 h, followed by administration with

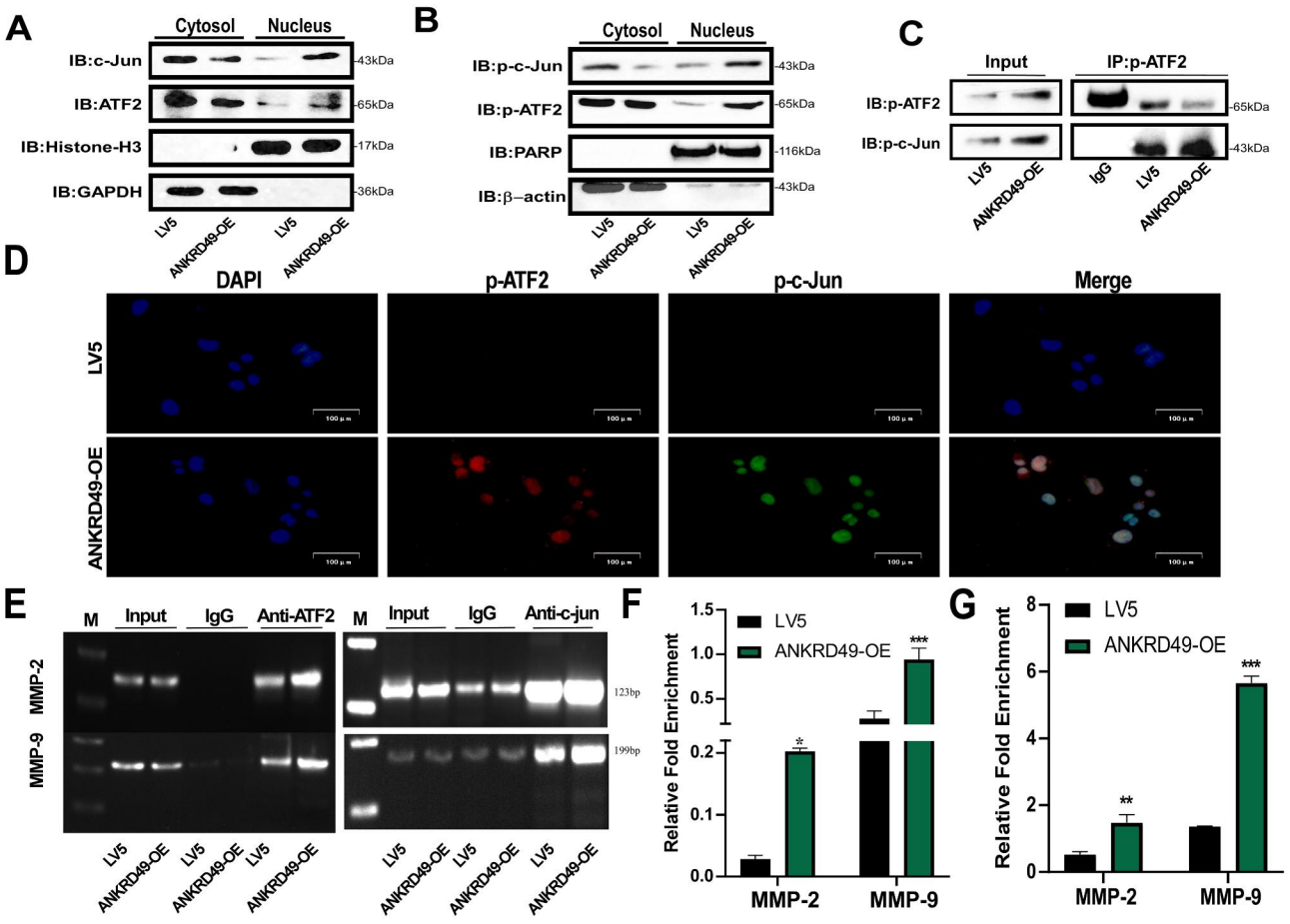

Fig. 5 ANKRD49 activates c-Jun/ATF2 transcription factor to regulate the expression of MMP-2/MMP-9 in H1299 cells. (**A**) The levels of ATF2 and c-Jun in the nuclear fraction of ANKRD49-OE or LV5 H1299 cells were measured by Western blot. (**B**) The levels of p-ATF2 and p-c-Jun in the nuclear fraction of ANKRD49-OE or LV5 H1299 cells were measured by Western blot. (**C**) Co-immunoprecipitation (Co-IP) analysis was performed to assess the interaction between p-ATF2 and p-c-Jun in the nucleus of ANKRD49-OE or vector H1299 cells. (**D**) Representative immunofluorescence images of ANKRD49 induced nuclear co-location of p-ATF2 and p-c-Jun. Scale bar:100 μm. (**E**-**G**) Chromatin immunoprecipitating (CHIP) assay was carried out to analyze the binding of p-ATF2 or p-c-Jun with the promoter of MMP-2 or MMP-9. GAPDH, β-actin, PARP and Histone-H3 served as the internal control for cytosol and nuclear fractions, respectively. Data are expressed as means ± standard deviation. $^{*}P < 0.05$, $^{**}P < 0.01$, $^{***}P < 0.001$ vs. LV5 group

SB203580, SP600125 or DMSO for another 24 h. We found that Anisomycin significantly augmented MMP-2/MMP-9 levels in SB203580-treated cells, whereas Anisomycin had no effect on MMP-2/MMP-9 expression in SP600125-treated cells (Fig. 7G, H). These data suggest that ANKRD49 promotes the invasion and migration of H1703 cells by enhancing MMP-2/MMP-9 expression mediated by the JNK rather than p38 MAPK pathway.

ANKRD49 potentiates migration and invasion of H1299 and H1703 cells in nude mice

To further explore the effect of ANKRD49 on the migration of NSCLC cells, ANKRD49-OE or LV5 H1299 cells and ANKRD49-sh or LV3 H1703 cells were injected intravenously into the tail of nude mice and maintained for 4 weeks. The results appeared that ANKRD49-OE enhanced the incidence of lung metastasis and the number of metastatic foci (Fig. 8A, B). Downregulation of ANKRD49 substantially reduced the incidence of lung metastasis and number of metastatic foci (Fig. 9A, B). Images of the mouse lungs are shown in Supplementary Fig. S5. HE staining also illustrated that more tumor cells appeared in perivascular and peribronchial regions in lung tissues from mice injected with ANKRD49-OE H1299 cells than in control mice (Fig. 8C). Nevertheless, the distribution of tumor cells in the lung tissues of mice injected with ANKRD49-sh or LV3 showed the opposite trend (Fig. 9C).

NAPSA and NKX2-1 are markers for LUAD [26–28], whereas p63 is a marker for LUSC [29]. Immunohistochemical staining illustrated that the distribution of ANKRD49-positive cells as well as NAPSA-positive, NKX2-1-positive, or p63-positive cells was consistent with the results of HE staining (Figs. 8D and 9D). In addition, immunohistochemical staining showed that the levels of ANKRD49, MMP-2, MMP-9, p-JNK, p-c-Jun,

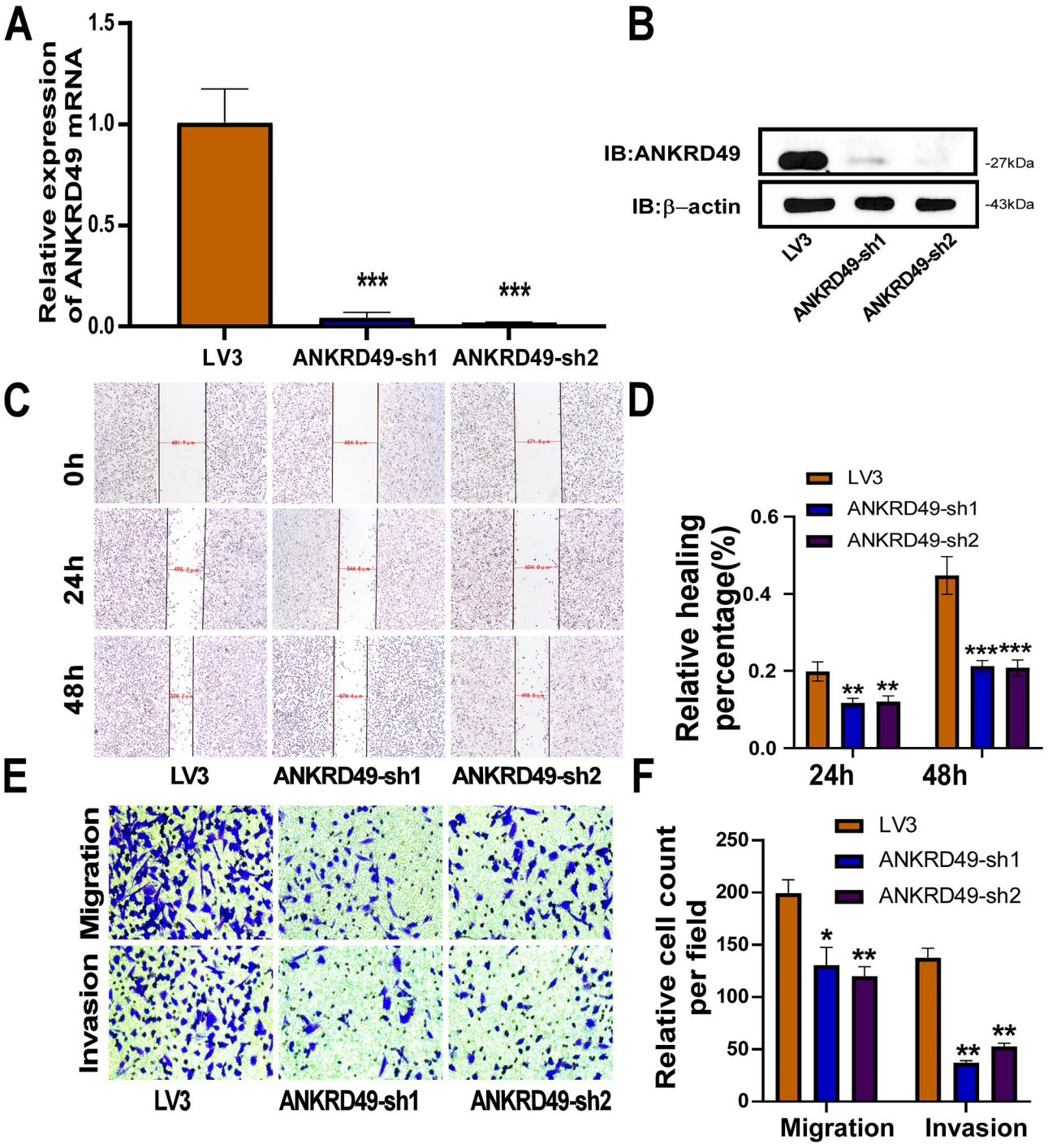

Fig. 6 Knockdown of ANKRD49 inhibits migration, invasion of H1703 cells. (**A**, **B**) The stable ANKRD49-sh H1703 cells was validated by RT-qPCR and Western blot. β-actin served as an internal control. (**C**, **D**) Wound healing assay was performed to detect migration of ANKRD49-sh H1703 cells, representative images were taken at 40× magnification at 0, 24 and 48 h. (**E**, **F**) Transwell migration and invasion assays were conducted to evaluate the migration and invasion of ANKRD49-sh H1703 cells. Representative images were taken at 200× magnification. Data are expressed as means ± standard deviation. $^{*}P < 0.05$, $^{**}P < 0.01$, $^{***}P < 0.001$ vs. LV3 group

and p-ATF2 were elevated in lung tissues from mice injected with ANKRD49-OE H1299 cells (Fig. 8E-G), whereas their levels were decreased in lung tissues of mice injected with ANKRD49-sh H1703 cells (Fig. 9E-G), compared to control mice. Correlation analysis displayed that the metastatic rates of the tumor cells were positively correlated with the expression of ANKRD49, MMP-2, MMP-9, p-JNK, p-c-Jun or p-ATF2 (Supplementary Fig.

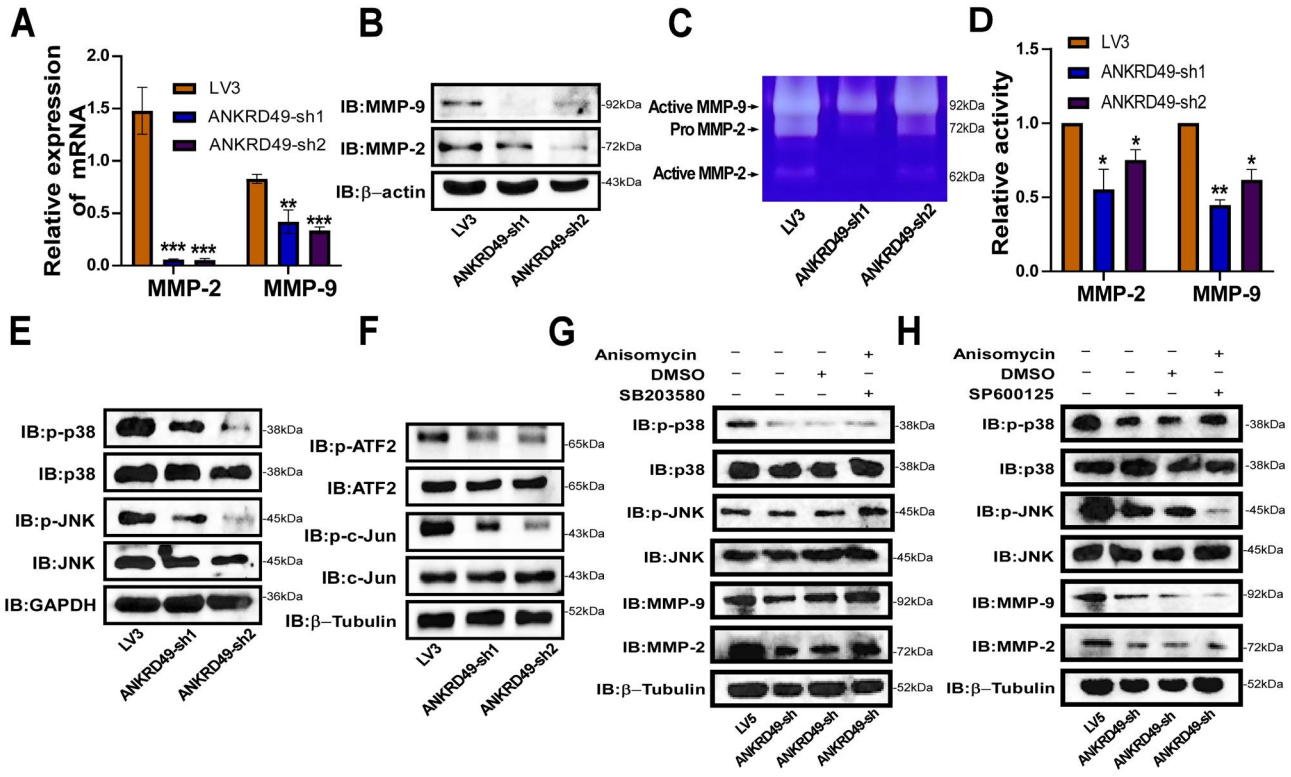

Fig. 7 Knockdown of ANKRD49 downregulates MMP-2/MMP-9 expression of H1703 cells. (**A**, **B**) The mRNA and protein levels of MMP-2 and MMP-9 in ANKRD49-sh H1703 cells were analyzed by RT-qPCR and Western blot. (**C**, **D**) The activities of MMP-2 and MMP-9 in ANKRD49-sh H1703 cells were detected by gelatin zymography. (**E**) The MAPK proteins in ANKRD49-sh H1703 cells were detected by Western blot. GAPDH served as an internal control. (**F**) The levels of p-ATF2 and p-c-Jun in ANKRD49-sh H1703 cells were measured by Western blot. (**G**, **H**) The levels of JNK, p-JNK, p38, p-p38, MMP-2 and MMP-9 in ANKRD49-sh H1703 cells treated with SP600125, SB203580, Anisomycin or DMSO were measured by Western blot. β-Tubulin served as an internal control. Data are expressed as means ± standard deviation. $^{*}P < 0.05$, $^{**}P < 0.01$, $^{***}P < 0.001$ vs. LV3 group

S6). In addition, MMP-2, MMP-9, p-JNK, p-ATF2, and p-c-Jun levels were positively correlated with the levels of ANKRD49 (Supplementary Fig. S7). In summary, ANKRD49 accelerated the invasion and metastasis of NSCLC cells via JNK-mediated transcription activation of c-Jun and ATF2 which regulated the expression of MMP-2/MMP-9.

Discussion

The ANKRD49 protein contains four ankyrin repeat motifs involved in multiple protein-protein interactions in diverse life activities [6]. It has been documented that ANKRD49 is highly expressed in several carcinomas, including gastric cancer and malignant gliomas. As an oncogene in malignant gliomas, ANKRD49 reduces cellular apoptosis and facilitates cell cycle progression to promote the proliferation of glioma cells. ANKRD49 can be an attractive therapeutic target for malignant glioma. [9]. It also has been documented that ANKRD49 may serve as an independent prognostic indicator of gastric cancer as it is highly expressed [8]. Similar results from a previous study showing ANKRD49, as one of the four gene signature from NCI-60 cell line, had a strong prediction value for non-small-cell lung cancer [30]. Our previous study using microarray analysis combined with IHC staining of tissue from 160 NSCLC patients, including 80 LUAD cases and 80 LUSC cases, showed that ANKRD49 is highly expressed in cancerous lung tissues and correlates with lymph node metastasis, distal metastasis, TNM stage, and differentiation in NSCLC patients. Furthermore, higher ANKRD49 expression was associated with poor OS in patients with NSCLC [10]. Another previous study from us showed that ANKRD49 promoted the invasion and migration of A549 cells via a P38 MAPK/ATF-2/MMPs signaling pathway in vitro and in vivo [11]. These data implied that ANKRD49 participates in the occurrence and development of NSCLC.

Previously, we used A549 cells, a LUAD cell line, to explore the function of ANKRD49. We found that ANKRD49 promoted the metastasis of A549 cells via upregulation of MMP- 2 and MMP- 9 in a P38/ATF- 2 pathway- dependent manner [11]. In consideration of different subtypes of NSCLC as well as heterogeneity of tumor cells, the function of ANKRD49 in NSCLC progression need further clarification. Herein, we used a lentivirus-mediated overexpression vector to upregulate

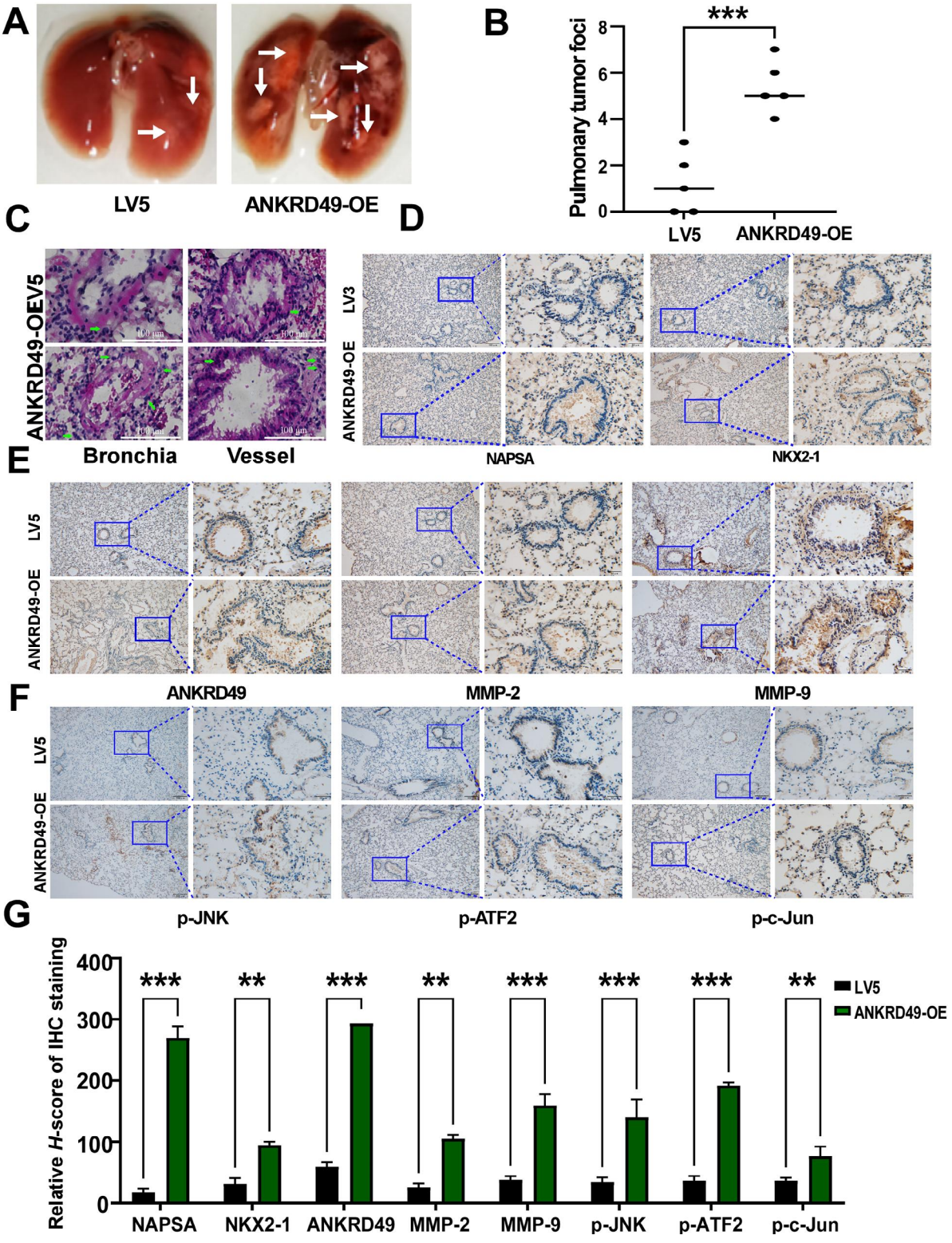

Fig. 8 Overexpression of ANKRD49 promotes the migration and invasion of H1299 cells in nude mice. (**A**) Representative lung images of mice injected with ANKRD49-OE-H1299 or LV5-H1299 cells. White arrows manifest the metastasis nodules on the lung. (**B**) Statistical analysis of the number of metastasis nodules on the lung was illustrated. (**C**) Representative images of HE staining for lung metastases. Green arrows indicated metastatic H1299 cells. (**D**) Representative images of IHC staining for NAPSA and NKX2-1. Scale bars represent 100 μm. (**E**, **F**) Representative images of IHC staining for ANKRD49, MMP-2, MMP-9, p-JNK, p-ATF2 or p-c-Jun. Scale bars represent 100 μm. (**G**) Quantitative analysis of IHC staining. $^{**}P < 0.01$, $^{***}P < 0.001$ vs. LV5 group

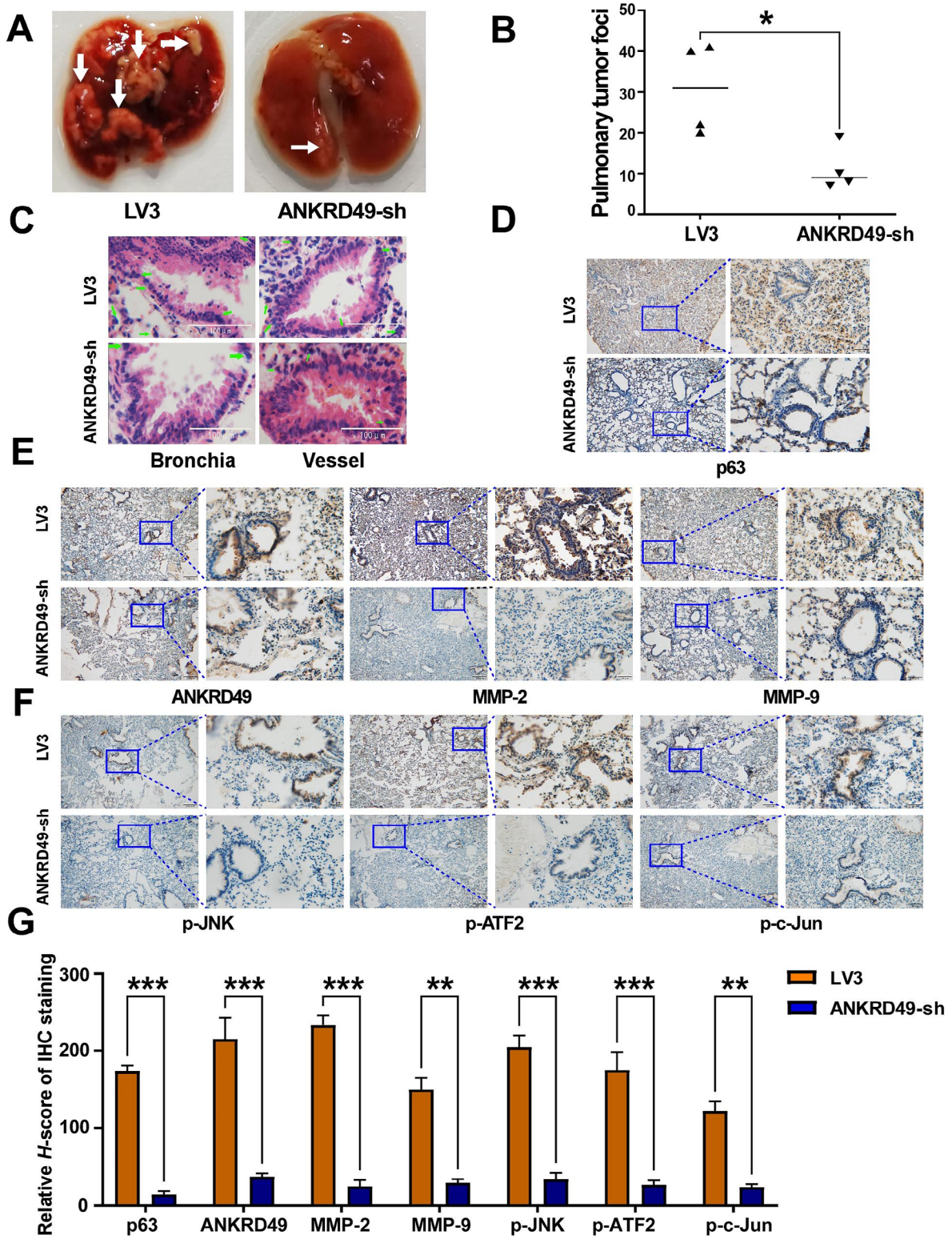

Fig. 9 Knockdown of ANKRD49 declines the migration and invasion of H1703 cells in nude mice. (**A**) Representative lung images of mice injected with ANKRD49-sh or LV3 H1703 cells. White arrows manifest the metastasis nodules on the lung. (**B**) Statistical analysis of the number of metastasis nodules on the lung was illustrated. (**C**) Representative images of HE staining for lung metastases. Green arrows indicated metastatic H1703 cells. (**D**) Representative images of IHC staining for p63. Scale bars represent 100 μm. (**E**, **F**) Representative images of IHC staining for ANKRD49, MMP-2, MMP-9, p-JNK, p-ATF2 or p-c-Jun. Scale bars represent 100 μm. (**G**) Quantitative analysis of IHC staining. $^{**}P < 0.01$, $^{***}P < 0.001$ vs. LV3 group

ANKRD49 expression in H1299 cells, another LUAD cell line, and found that ANKRD49 potentiated the invasion and metastasis of H1299 cells. Furthermore, we utilized lentivirus-mediated shRNA, a loss-of-function strategy, to downregulate ANKRD49 expression in H1299 and H1703 cells (a LUSC cell line), and discovered that knockdown of ANKRD49 suppressed the invasion and migration of these cancer cells. Importantly, we also found that differential endogenous levels of ANKRD49 in H1299 and H1703 cells also have correspondingly differential migration and invasion (supplemental Fig. S3). The migration and invasion of cancer cells into surrounding tissues and vasculature are the crucial initial step in tumor metastasis, enabling the tumor to colonize distant organs [31]. It is widely acknowledged that metastasis is a key cause of cancer-related death, and cell migration is a sophisticated multistep process [32]. During this multistep process, degradation of the extracellular matrix (ECM) is an early event in tumor metastasis [33]. MMPs belong to a family of proteolytic enzymes with many physiological roles, including ECM modification, which accelerates cell migration [34]. Among the MMP family, MMP-2 and MMP-9 are documented as substrate-specific gelatinases that are pivotal in ECM degradation [35] and are advantageous for invasion and metastasis of tumor cells, leading to tumorigenesis [36]. Our study demonstrated that ANKRD49 promotes the expression and activity of MMP-2 and MMP-9, which enhances the migration and invasion of NSCLC cells.

The JNK and p38 MAPK signaling pathways are characterized by kinase cascades in cancer biology and play a central role in the carcinogenesis and maintenance of cancers [37, 38]. JNK and p38 MAPK have been identified as crucial mediators of migration and invasion in various tumors [39, 40]. In this study, the phosphorylation of JNK and p38 was elevated in ANKRD49 ectopic expressed H1299 cells and decreased in ANKRD49 downregulated H1299 and H1703 cells. So, we speculated that the JNK and p38 MAPK pathways were involved in ANKRD49-induced cellular migration and invasion. However, unlike the JNK inhibitor, the p38 MAPK inhibitor did not induce a decline in the levels of MMP-2 and MMP-9. These data demonstrate that the JNK signaling pathway participates in ANKRD49-induced migration and invasion of H1299 and H1703 cells. Activated p38 signaling pathway may or may not contribute to tumor immunity [41] rather than metastasis in current settings. The present results were inconsistent with those in A549 cells, a possible reason was that these three types of cell lines have diverse genetic and histological backgrounds. A549 cells have been tested for the KRAS and KEAP1 (kelch like ECH associated protein 1) missense mutation, STK11 (serine/threonine kinase 11) nonsense mutation, wild type p53 expression, while H1299 cells have a homozygous partial deletion of the p53 protein, and lack expression of p53 protein [42]. Of course, how these different genetic backgrounds affect p38 signaling pathway remains to be further studied.

Subsequently, we sought to understand how JNK regulates MMP-2 and MMP-9 expression. MMP-2 or MMP-9 transcription is reportedly regulated by various transcription factors, including AP-1, SP-1, NF-κB, and CREB [43]. ATF2 and c-Jun are components of the dimeric transcription factor AP-1 and play crucial regulatory roles in many biological processes [44]. Both ATF2 and c-Jun can be phosphorylated by JNK and subsequently translocated into the nucleus to function as transcription factors [45]. The phosphorylation of ATF2 and c-Jun, as well as their nuclear distribution, were elevated in ANKRD49 overexpressed H1299 cells, and downregulation of ANKRD49 inhibited this tendency. It has been reported that in the absence of c-Jun, the monomers of ATF2 continuously shuttle between the nucleus and cytoplasm because it contains a nuclear export signal (NES) and two nuclear localization sequences (NLS), while the homodimers of ATF2 are predominantly distributed in the cytoplasm [46]. To function as a transcription factor, ATF2 needs to form a heterodimer with c-Jun, which masks NES and prevents ATF2 nuclear export [47]. Herein, we found that ANKRD49 boosted the interaction between ATF2 and c-Jun in the nucleus through Co-IP and immunofluorescence staining assays. It is well established that the promoter of MMP-2/MMP-9 contains the binding site of c-Jun [48], yet the binding sites of ATF2 in the promoter region of MMP-2 and MMP-9 have not been revealed. In the present study, a CHIP assay was carried out, and it was discovered that ATF2 binding sites exist in -1795~-1788 of the MMP-2 promoter region and −2042~-2395 of the MMP-9 promoter region. ANKRD49 facilitated binding of ATF2 to the promoter regions of MMP-2 and MMP-9. In the end, our in vitro tests confirmed the ANKRD49's function. Consequently, we conclude that ANKRD49 mediates MMP-2/MMP-9 via ATF2/c-Jun heterodimers, which are activated by JNK to promote the migration and invasion of NSCLC cells. Of course, apart from MMPs and MAPKs, other mechanisms such as epithelial-to-mesenchymal transition (EMT), angiogenesis or the stemness of tumor cells may be invovled in ANKRD49's function on migration and invasion of NSCLC cells. Therefore, a more comprehensive mechanism will be investigated in our future work.

Interestingly, a recent study demonstrated that ANKRD49 expression is positively correlated to glioma grade and manifests a significant prognosis difference between glioma samples and non-glioma samples, suggesting that ANKRD49 may serve as a prognosis predictor [8]. Similar results from our previous study showed that ANKRD49 protein in LUSC was elevated and

correlated positively with the tumor node-metastasis stage, lymph node metastasis, distal metastasis, and differentiation. Patients with higher ANKRD49 had lower overall survival rate and higher ANKRD49 expression in lung tissues may be used as an independent prognostic marker for LUSC patients [10]. These results indicated that ANKRD49 could be a potential pan-cancer predictor. Our study defines a mechanism for ANKRD49 in acceleration of invasion and metastasis of NSCLC cells (Fig. 10). In turn, inactivating the JNK-ATF2/c-Jun pathways inhibit NSCLC metastasis. Therefore, ANKRD49 may serve as a potential anti-metastatic therapeutic target and a novel prognostic biomarker for NSCLC.

The present study has several unaddressed issues. The role of activated p38 MAPK in ANKRD49-OE H1299 or ANKRD49-sh H1703 cells remains unclear. The mechanism by which ANKRD49 establishes contact with JNK or p38 MAPK remains unknown. Accordingly, more in-depth research is needed to elucidate the function and underlying mechanisms of ANKRD49 in NSCLC progression.

Conclusions

We found that ANKRD49 potentiates the migration and invasion of H1299 and H1703 cells by activating the JNK-ATF2/c-Jun signaling cascade to upregulate MMP2 and MMP-9 expression.

Abbreviations

NSCLC	non-small cell lung cancer
LUAD	lung adenocarcinoma
LUSC	lung squamous cell carcinoma
ANKRD49	ankyrin repeat domain 49
shRNA	short hairpin RNA
MMP	matrix metalloproteinase
ECM	extracellular matrix
MAPK	mitogen-activated protein kinase
ERK	signal-regulated kinases
JNK	c-Jun N-terminal kinase
ATF2	activating transcription factor 2
CO-IP	co-immunoprecipitation
CHIP	chromatin immunoprecipitation
LV	lentivirus
CCK-8	cell counting kit-8
DNA	deoxyribonucleic acid
PCR	polymerase chain reaction
SYBR	synergy brands
GAPDH	glyceraldehyde-3-phosphate dehydrogenase
IHC	immunohistochemistry
RT-qRCR	Real-time quantitative PCR
BCA	bicinchoninic acid
SDS-PAGE	sodium dodecyl sulfate polyacrylamide gel electrophoresis
PVDF	poly vinylidene fluoride membrane
NES	nuclear export signal
NLS	nuclear localization sequence
DAPI	diamidino-phenyl-indole
SPF	Specific Pathogen Free
KEAP1	kelch like ECH associated protein 1
STK11	serine/threonine kinase 11

Supplementary Information

The online version contains supplementary material available at https://doi.org/10.1186/s12885-023-11612-9.

Additional file 1. Additional Figures

Additional file 2. Additional Tables

Additional file 3. Original Data

Acknowledgements

We thank Home for Researchers (www.home-for-researchers.com) for correcting the grammar and spelling.

Authors' contributions

MP and HW conceived and designed the project. JS, JH, CL completed the experiments and analyzed the data. YL collected the human samples. MG, RF and WW analyzed the data from animal experiments. JS and JH wrote the manuscript. HW provided advice and critical comments. The MP was responsible for research supervision and funding acquisition. All authors have read and approved the final manuscript.

Funding

This work was supported by funding from the Science and Technology Cooperation and Exchange Special Project of Shanxi Province (No. 202104041101012), the Natural Science Fund of Shanxi Province (No. 202201D111352), the Non-profit Central Research Institute Fund of Chinese Academy of Medical Science (No.2020-PT320-005).

Data Availability

All materials are available by contacting the corresponding author.

Declarations

Ethics approval and consent to participate

All tissue samples were obtained in accordance with the Declaration of Helsinki (1975) and were approved by the ethics committee of the First Hospital of Shanxi Medical University (approval number 2019K042). All procedures performed in studies involving human participants were performed per the ethical standards of the institution with written and verbal informed consent. All experiments in this study were performed in accordance with relevant guidelines and regulations and were approved by Ethics Committee of Shanxi Medical University. All animal experiments were approved by the Animal Ethics Committee of the Shanxi Medical University (approval number SYDL-2020016) and was performed according to the procedures that complied with the ARRIVE guidelines.

Consent for publication

Not applicable for this article.

Competing interests

The authors declare that they have no competing interests.

Author details

[1]Department of Pulmonary and Critical Care Medicine, Shanxi Province Key Laboratory of Respiratory Disease, the First Hospital, Shanxi Medical University, NHC Key Laboratory of Pneumoconiosis, Taiyuan, Shanxi 030001, China
[2]Department of Laboratorial Medicine, Changzhi Traditional Chinese Medicine Hospital, Changzhi 046000, China
[3]School of Basic Medicine, Basic Medical Sciences Center, Shanxi Medical University, No. 55 Wenhua Street, Jinzhong, Shanxi 030600, China
[4]Department of Respiratory Medicine 1, Shanxi Hospital Affiliated to Cancer Hospital, Shanxi Province Cancer Hospital, Chinese Academy of Medical Sciences, Cancer Hospital Affiliated to Shanxi Medical University, Taiyuan, Shanxi 030013, China
[5]Laboratory of Animal Center, Shanxi Medical University, Taiyuan 030001, China

[6]Department of Pulmonary and Critical Care Medicine, the First Hospital, Shanxi Medical University, No. 85 Jiefang South Road, Taiyuan, Shanxi 030001, China

Received: 7 April 2023 / Accepted: 4 November 2023
Published online: 14 November 2023

References

1. Bray F, Ferlay J, Soerjomataram I, Siegel RL, Torre LA, Jemal A. Global cancer statistics 2018: GLOBOCAN estimates of incidence and mortality worldwide for 36 cancers in 185 countries. CA Cancer J Clin. 2018;68(6):394–424.
2. Keating GM. Nivolumab: a review in advanced squamous non-small cell Lung cancer. Drugs. 2015;75(16):1925–34.
3. Huang T, Li J, Zhang C, Hong Q, Jiang D, Ye M, Duan S. Distinguishing lung adenocarcinoma from lung squamous cell carcinoma by two hypomethylated and three hypermethylated genes: a Meta-analysis. PLoS ONE. 2016;11(2):e0149088.
4. Rosell R, Karachaliou N. Lung cancer: maintenance therapy and precision medicine in NSCLC. Nat Rev Clin Oncol. 2013;10(10):549–50.
5. MacDonagh L, Gray SG, Breen E, Cuffe S, Finn SP, O'Byrne KJ, Barr MP. BBI608 inhibits cancer stemness and reverses cisplatin resistance in NSCLC. Cancer Lett. 2018;428:117–26.
6. Wang HL, Fan SS, Pang M, Liu YH, Guo M, Liang JB, Zhang JL, Yu BF, Guo R, Xie J, et al. The ankyrin repeat domain 49 (ANKRD49) augments autophagy of serum-starved GC-1 cells through the NF-κB pathway. PLoS ONE. 2015;10(6):e0128551.
7. Zhou X, Wang WT, Sun J, Liu HY, Bai XY, Liu JJ, Yu BF, Guo R, Wang HL. ANKRD49 inhibits etoposide-induced intrinsic apoptosis of GC-1 cells by modulating NF-κB signaling. Mol Cell Biochem. 2019;457(1–2):21–9.
8. Liu CG, Cui XL, Wei ZG, Guo JS. High expression of the ANKRD49 protein is associated with progression and poor prognosis of gastric cancer. Cancer Biomark. 2018;22(4):649–56.
9. Hao C, Duan H, Li H, Pei M, Liu Y, Fan Y, Zhang C. Up-regulation of ANKDR49, a poor prognostic factor, regulates cell proliferation of gliomas. Biosci Rep 2017, 37(4).
10. Li XY, Qin KR, Liu YH, Pang M, Huo YK, Yu BF, Wang HL. A microarray study on the expression of ANKRD49 in lung squamous cell carcinoma and its clinicopathologic significance. Appl Immunohistochem Mol Morphol. 2022;30(6):418–24.
11. Liu YH, Yuan M, Xu BX, Gao R, You YJ, Wang ZX, Zhang YC, Guo M, Chen ZY, Yu BF, et al. ANKRD49 promotes the invasion and Metastasis of lung adenocarcinoma via a P38/ATF-2 signalling pathway. J Cell Mol Med. 2022;26(16):4401–15.
12. Wang X, Yang B, She Y, Ye Y. The lncRNA TP73-AS1 promotes Ovarian cancer cell proliferation and Metastasis via modulation of MMP2 and MMP9. J Cell Biochem. 2018;119(9):7790–9.
13. Xu F, Li Q, Wang Z, Cao X. Sinomenine inhibits proliferation, migration, invasion and promotes apoptosis of Prostate cancer cells by regulation of miR-23a. Biomed Pharmacother. 2019;112:108592.
14. Feng X, Yan N, Sun W, Zheng S, Jiang S, Wang J, Guo C, Hao L, Tian Y, Liu S, et al. Mir-4521-FAM129A axial regulation on ccRCC progression through TIMP-1/MMP2/MMP9 and MDM2/p53/Bcl2/Bax pathways. Cell Death Discov. 2019;5:89.
15. Zhou Z, Zhou Q, Wu X, Xu S, Hu X, Tao X, Li B, Peng J, Li D, Shen L, et al. VCAM-1 secreted from cancer-associated fibroblasts enhances the growth and invasion of Lung cancer cells through AKT and MAPK signaling. Cancer Lett. 2020;473:62–73.
16. Li S, Mai H, Zhu Y, Li G, Sun J, Li G, Liang B, Chen S. MicroRNA-4500 inhibits Migration, Invasion, and angiogenesis of Breast Cancer cells via RRM2-Dependent MAPK signaling pathway. Mol Ther Nucleic Acids. 2020;21:278–89.
17. Wei CH, Wu G, Cai Q, Gao XC, Tong F, Zhou R, Zhang RG, Dong JH, Hu Y, Dong XR. MicroRNA-330-3p promotes cell invasion and Metastasis in non-small cell Lung cancer through GRIA3 by activating MAPK/ERK signaling pathway. J Hematol Oncol. 2017;10(1):125.
18. Min BW, Kim CG, Ko J, Lim Y, Lee YH, Shin SY. Transcription of the protein kinase C-delta gene is activated by JNK through c-Jun and ATF2 in response to the anticancer agent doxorubicin. Exp Mol Med. 2008;40(6):699–708.
19. Li M, Zhang D, Ge X, Zhu X, Zhou Y, Zhang Y, Peng X, Shen A. TRAF6-p38/JNK-ATF2 axis promotes microglial inflammatory activation. Exp Cell Res. 2019;376(2):133–48.
20. Meng Q, Xia Y. c-Jun, at the crossroad of the signaling network. Protein Cell. 2011;2(11):889–98.
21. Liu JF, Chen PC, Chang TM, Hou CH. Monocyte chemoattractant Protein-1 promotes cancer cell migration via c-Raf/MAPK/AP-1 pathway and MMP-9 production in osteosarcoma. J Exp Clin Cancer Res. 2020;39(1):254.
22. Oh JH, Joo YH, Karadeniz F, Ko J, Kong CS. Syringaresinol inhibits UVA-Induced MMP-1 expression by suppression of MAPK/AP-1 signaling in HaCaT keratinocytes and human dermal fibroblasts. Int J Mol Sci 2020, 21(11).
23. Lau E, Ronai ZA. ATF2 - at the crossroad of nuclear and cytosolic functions. J Cell Sci. 2012;125(Pt 12):2815–24.
24. Gozdecka M, Breitwieser W. The roles of ATF2 (activating transcription factor 2) in tumorigenesis. Biochem Soc Trans. 2012;40(1):230–4.
25. Wang Y, Gao H, Cao X, Li Z, Kuang Y, Ji Y, Li Y. Role of GADD45A in myocardial ischemia/reperfusion through mediation of the JNK/p38 MAPK and STAT3/VEGF pathways. Int J Mol Med 2022, 50(6).
26. Wu J, Zhang Y, Ding T, Cheng R, Gong W, Guo Y, Luo Y, Pan Y, Zhai Q, Sun W, et al. Napsin A expression in subtypes of thyroid tumors: comparison with Lung Adenocarcinomas. Endocr Pathol. 2020;31(1):39–45.
27. Yang L, Lin M, Ruan WJ, Dong LL, Chen EG, Wu XH, Ying KJ. Nkx2-1: a novel Tumor biomarker of Lung cancer. J Zhejiang Univ Sci B. 2012;13(11):855–66.
28. Jones RA, Franks SE, Moorehead RA. Comparative mRNA and miRNA transcriptome analysis of a mouse model of IGFIR-driven Lung cancer. PLoS ONE. 2018;13(11):e0206948.
29. Nobre AR, Albergaria A, Schmitt F. p40: a p63 isoform useful for Lung cancer diagnosis - a review of the physiological and pathological role of p63. Acta Cytol. 2013;57(1):1–8.
30. Hsu YC, Yuan S, Chen HY, Yu SL, Liu CH, Hsu PY, Wu G, Lin CH, Chang GC, Li KC, et al. A four-gene signature from NCI-60 cell line for survival prediction in non-small cell Lung cancer. Clin cancer Research: Official J Am Association Cancer Res. 2009;15(23):7309–15.
31. Duff D, Long A. Roles for RACK1 in cancer cell migration and invasion. Cell Signal. 2017;35:250–5.
32. Polacheck WJ, Zervantonakis IK, Kamm RD. Tumor cell migration in complex microenvironments. Cell Mol Life Sci. 2013;70(8):1335–56.
33. Mikami S, Oya M, Mizuno R, Kosaka T, Katsube K, Okada Y. Invasion and Metastasis of renal cell carcinoma. Med Mol Morphol. 2014;47(2):63–7.
34. Wells JM, Gaggar A, Blalock JE. MMP generated matrikines. Matrix Biol. 2015;44–46:122–9.
35. Yang HL, Thiyagarajan V, Shen PC, Mathew DC, Lin KY, Liao JW, Hseu YC. Anti-EMT properties of CoQ0 attributed to PI3K/AKT/NFKB/MMP-9 signaling pathway through ROS-mediated apoptosis. J Exp Clin Cancer Res. 2019;38(1):186.
36. Jacob A, Jing J, Lee J, Schedin P, Gilbert SM, Peden AA, Junutula JR, Prekeris R. Rab40b regulates trafficking of MMP2 and MMP9 during invadopodia formation and invasion of Breast cancer cells. J Cell Sci. 2013;126(Pt 20):4647–58.
37. Wagner EF, Nebreda AR. Signal integration by JNK and p38 MAPK pathways in cancer development. Nat Rev Cancer. 2009;9(8):537–49.
38. Aggarwal V, Tuli HS, Varol A, Thakral F, Yerer MB, Sak K, Varol M, Jain A, Khan MA, Sethi G. Role of reactive oxygen species in Cancer Progression: Molecular mechanisms and recent advancements. Biomolecules 2019, 9(11).
39. Wang J, Liu Q, Xiao H, Luo X, Liu X. Suppressive effects of Momordin Ic on HepG2 cell migration and invasion by regulating MMP-9 and adhesion molecules: involvement of p38 and JNK pathways. Toxicol in Vitro. 2019;56:75–83.
40. Ou S, Liao Y, Shi J, Tang J, Ye Y, Wu F, Wang W, Fei J, Xie F, Bai L. S100A16 suppresses the proliferation, migration and invasion of Colorectal cancer cells in part via the JNK/p38 MAPK pathway. Mol Med Rep 2021, 23(2).
41. Lin Z, Huang Q, Liu J, Wang H, Zhang X, Zhu Z, Zhang W, Wei Y, Liu Z, Du W. Interleukin-17D promotes Lung cancer progression by inducing tumor-associated macrophage infiltration via the p38 MAPK signaling pathway. Aging. 2022;14(15):6149–68.
42. Hinz TK, Kalkur R, Rabinovitch J, Hinkle W, Heasley LE. TP53 null mutations identify Lung Cancer Cell lines with highest sensitivity to the nontaxane microtubule inhibitor eribulin. Mol Pharmacol. 2021;100(2):144–54.
43. Li S, Ung TT, Nguyen TT, Sah DK, Park SY, Jung YD. Cholic Acid stimulates MMP-9 in human Colon Cancer cells via activation of MAPK, AP-1, and NF-κB activity. Int J Mol Sci 2020, 21(10).
44. Lopez-Bergami P, Lau E, Ronai Z. Emerging roles of ATF2 and the dynamic AP1 network in cancer. Nat Rev Cancer. 2010;10(1):65–76.

45. Pant I, Rao SG, Kondaiah P. Role of areca nut induced JNK/ATF2/Jun axis in the activation of TGF-β pathway in precancerous oral Submucous Fibrosis. Sci Rep. 2016;6:34314.
46. Watson G, Ronai ZA, Lau E. ATF2, a paradigm of the multifaceted regulation of transcription factors in biology and Disease. Pharmacol Res. 2017;119:347–57.
47. Lindaman LL, Yeh DM, Xie C, Breen KM, Coss D. Phosphorylation of ATF2 and interaction with NFY induces c-Jun in the gonadotrope. Mol Cell Endocrinol. 2013;365(2):316–26.
48. Tombulturk FK, Soydas T, Sarac EY, Tuncdemir M, Coskunpinar E, Polat E, Sirekbasan S, Kanigur-Sultuybek G. Regulation of MMP 2 and MMP 9 expressions modulated by AP-1 (c-jun) in wound healing: improving role of Lucilia Sericata in diabetic rats. Acta Diabetol. 2019;56(2):177–86.

Publisher's Note